

pubs.acs.org/Macromolecules Article

# Analysis of Surface Segregation of Bottlebrush Polymer Additives in Thin Film Blends with Attractive Intermolecular Interactions

Kazuma Miyagi, Hao Mei, Tanguy Terlier, Gila E. Stein,\* and Rafael Verduzco\*



Cite This: Macromolecules 2020, 53, 6720-6730



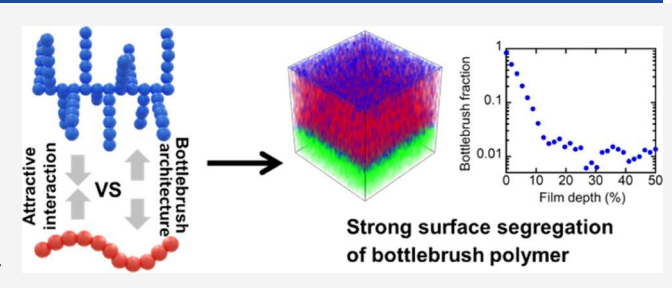
**ACCESS** 

Metrics & More

Article Recommendations

Supporting Information

**ABSTRACT:** The surface chemistry of polymer films and coatings is relevant to a wide range of applications, and recent work has shown that bottlebrush polymers can be used as additives to modify film interfaces and surfaces. In blends with linear polymers of a sufficient molecular weight, bottlebrush polymers will enrich interfaces driven, in part, by entropic effects. However, prior work has only studied a limited set of systems with either neutral or repulsive interactions between the bottlebrush and linear polymers. Herein, we investigated surface segregation in blends of bottlebrush and linear polymers with attractive intermolecular



interactions. Specifically, we studied blends of bottlebrush poly(cyclohexyl methacrylate) (BBPCHMA) and linear polystyrene (PS) over a range of BBPCHMA backbone and linear PS lengths. Time-of-flight secondary ion mass spectroscopy measurements of the blends showed that bottlebrush additives strongly segregated to the film surface when the bottlebrush side chain was shorter than matrix linear PS, and the surface remained enriched with bottlebrush after 2 days of thermal annealing. In comparison to studies with bottlebrushes having neutral or repulsive interactions with linear PS, the surface segregation of BBPCHMA was weaker in the as-cast films but more significant after thermal annealing. This comparison suggests that architectural effects can drive segregation during casting and the interaction of the polymers with the air interface is more significant during thermal annealing. Finally, we demonstrated that these bottlebrush additives could self-heal a damaged surface by diffusing to a damaged region during thermal annealing. This work provides new insight into the segregation behavior of bottlebrush polymer additives and factors that drive segregation during casting and thermal annealing.

## ■ INTRODUCTION

The surface chemistry of polymer films and coatings is relevant to a wide range of applications including antifouling materials, <sup>1–3</sup> organic electronic devices, <sup>4–6</sup> bio-interfaces, <sup>7–9</sup> and surface friction. <sup>10–13</sup> In blend films and coatings, a combination of enthalpic, entropic, and kinetic effects can drive surface segregation or enrichment of one component, even when the blends are fully miscible. <sup>14</sup> Enthalpic effects will preferentially drive polymers with low cohesive energy densities to the surface, and these effects have been leveraged to produce low-energy antifouling surfaces. <sup>15–18</sup> Entropic effects will preferentially drive shorter, more branched, or more rigid polymers to surfaces and interfaces. <sup>19–29</sup> Kinetic effects also play a role in driving surface segregation in blends and depends on the solvent evaporation rate and relative sizes of solutes, among other factors. <sup>30–34</sup>

Bottlebrush polymers are branched polymers with a high density of polymeric side chains grafted to a linear backbone and are effective additives for modifying surfaces and interfaces by leveraging entropically mediated segregation. In blends with linear polymers, they exhibit preferential segregation to surfaces and interfaces when the side chains are shorter than the linear polymers. This segregation is driven, in part, by entropic effects, and a variety of surface-active bottlebrush

polymer additives have been demonstrated.<sup>35–39</sup> Bottlebrush polymers are also excellent model systems for studying surface segregation because the length and number of side-chains can be precisely controlled, enabling systematic analysis of the relationship between molecular architecture and surface activity.

Prior studies by us focused exclusively on blend systems with repulsive<sup>35</sup> or approximately neutral interactions<sup>36,37</sup> between the bottlebrush and linear polymer and found that repulsive interactions favored segregation and surface enrichment of the bottlebrush additives. For example, a much higher surface excess was observed for bottlebrush polymers with repulsive interactions with linear polystyrene (PS) compared with approximately neutral interactions. Specifically, bottlebrushes with a mixture of PS and poly(methyl methacrylate) (PMMA) side-chains<sup>35</sup> segregated to the surface more strongly than

Received: March 30, 2020 Revised: June 3, 2020 Published: July 29, 2020





Table 1. Characteristics of Bottlebrush Polymers with PCHMA Side Chains (BBPCHMA) Prepared for This Study<sup>a</sup>

sample name	[MM]/[cat]	$M_{\rm n}^{\ b}$ (kg/mol)	$\mathcal{D}^{c}$	$N_{\rm sc}^{d}$	$N_{ m b}^{\;m e}$	$N_{ m b}/N_{ m sc}$	$ ho^f$ (%)
BBPCHMA-25	50/1	198	1.30	44	25	0.57	89.6
BBPCHMA-62	100/1	491	1.54	44	62	1.4	80.1
BBPCHMA-95	200/1	744	1.53	44	95	2.2	78.9

"[MM]/[cat] is the ratio of the macromonomer to the catalyst,  $M_{\rm n}$  is the number-averaged molecular weight, D is molecular-weight dispersity,  $N_{\rm sc}$  is side-chain degree of polymerization,  $N_{\rm b}$  is the backbone degree of polymerization, and  $\rho$  indicates the conversion of the NBPCHMA macromonomer, as determined through GPC-RI analysis of the final product. Determined by GPC-LS analysis. Determined by GPC-RI analysis. Determined by GPC-RI analysis.

bottlebrushes with only PS side-chains<sup>36,37</sup> because the repulsive interactions favored depletion of the additive from the bulk

Prior work with blends of linear and branched polymer additives with attractive intermolecular interactions have found that entropic effects can drive the branched polymer to the film surface. Mayes and co-workers studied blends of linear PMMA and a branched random copolymer of methyl methacrylate and methoxy poly(ethylene glycol) monomethacrylate (P(MMA-r-MnG)) and showed that the branched polymer migrated to the film surface in thermally annealed films, while linear poly-(ethylene glycol) additives were depleted from the film surface due to repulsive interactions with the interface.<sup>3</sup> The segregation was attributed to configurational entropic effects which drive chain ends toward interfaces. However, this study was limited to one branched polymer additive with relatively short side-chains (470 g/mol) in blends with high-molecular weight linear polymers (greater than 200 kg/mol) and to thermally annealed films. Simulations have been performed to study a wider parameter space of branched and linear polymer blends with attractive intermolecular interactions and predicted segregation of branched polymer additives. 23,40 For example, using self-consistent field theory, Walton and Mayes showed that both branched polymer and linear polymer additives can segregate to surfaces, even when the surface is repulsive to the additive, and that the branched polymer additives segregated to the surface over a wider range of additive molecular weights relative to linear polymer additives.<sup>23</sup> Yethiraj analyzed blends of linear and branched polymers using a tangent sphere model in which the branched and linear polymers were made up of the same number of identical beads. He found that segregation or depletion was driven by molecular packing effects, and attractive interactions between the beads resulted in segregation of the branched polymer to the surface due to the more efficient intermolecular packing of the linear chains. 40 However, experimental data of attractive blend systems and non-equilibrium effects are

The goal of this study was to investigate surface segregation in blends of bottlebrush and linear polymers with attractive intermolecular interactions in both the as-cast and thermally annealed films and with linear polymers either shorter or longer than the bottlebrush side-chain length. We focused on the fully miscible system of poly(cyclohexyl methacrylate) (PCHMA) and PS.  $^{41-43}$  We synthesized bottlebrush polymers (termed BBPCHMA) with PCHMA side chains and then prepared a series of BBPCHMA/PS blends that varied in bottlebrush backbone polymerization degree  $N_{\rm b}$  and the molecular weight of the linear polymer  $N_{\rm m}$ . We performed time-of-flight secondary ion mass spectroscopy (ToF-SIMS) depth-profiling analysis on all blended films to determine the bottlebrush distribution and detect segregation of the

bottlebrush polymer at the polymer—air and polymer—silicon interfaces. We found that BBPCHMA additives segregated to the free surface for a wide range of blend formulations and casting conditions. Through analysis of the bottlebrush distribution in the various samples and in both as-cast and thermally annealed films, we were able to gain insight into the enthalpic, entropic, and kinetic effects that drive segregation. We also compared the results of the attractive blends studied here to those of previously reported blends with neutral and repulsive interactions, and this comparison provided new insight into the factors that drive segregation during solution casting and subsequent thermal annealing. In addition, we found that bottlebrush surface layers removed by etching could be subsequently recovered by thermal annealing due to diffusion of bottlebrushes to the damaged site.

#### **EXPERIMENTAL SECTION**

Materials. All chemical reagents were purchased from commercial sources and used as received unless noted otherwise. Silicon wafers were washed by Hellmanex III, deionized water, acetone, and isopropyl alcohol with sonication for 15 min for each solvent and treated with UV/ozone for 40 min to remove contaminants. 2,2'azobis(2-methylpropionitrile) (AIBN) was purified by recrystallization in methanol. Cyclohexyl methacrylate (CHMA) (Sigma-Aldrich Co. LLC) was passed through an alumina column to remove the inhibitor. The 3rd generation Grubbs catalyst, dichloro [1,3-bis(2,4,6trimethylphenyl)-2-imidazolidinylidene](benzylidene)bis(3bromopyridine)ruthenium(II) was purchased from Sigma-Aldrich Co. LLC. Exo-5-nobornene-2-methanol (*exo*-NBOH)<sup>44</sup> and ((1*S*,2*R*,4*S*)bicyclo[2.2.1] hept-5-en-2-yl) methyl-4-cyano-4-(((dodecylsulfanyl)-4-cyano-4-(((dodecylsulfanyl)-4-cyano-4-(((dodecylsulfanyl)-4-cyano-4-(((dodecylsulfanyl)-4-cyano-4-(((dodecylsulfanyl)-4-cyano-4-(((dodecylsulfanyl)-4-cyano-4-(((dodecylsulfanyl)-4-cyano-4-(((dodecylsulfanyl)-4-cyano-4-(((dodecylsulfanyl)-4-cyano-4-(((dodecylsulfanyl)-4-cyano-4-(((dodecylsulfanyl)-4-cyano-4-(((dodecylsulfanyl)-4-cyano-4-(((dodecylsulfanyl)-4-cyano-4-(((dodecylsulfanyl)-4-cyano-4-((dodecylsulfanyl)-4-cyano-4-((dodecylsulfanyl)-4-cyano-4-((dodecylsulfanyl)-4-cyano-4-((dodecylsulfanyl)-4-cyano-4-((dodecylsulfanyl)-4-cyano-4-((dodecylsulfanyl)-4-cyano-4-(dcarbonothioyl)-thio)-pentanoate (NBCTA)35 were synthesized as previously reported. Linear PS polymers were purchased from Polymer Standard Service-USA Inc. Hydroxy-terminated PS with weight-average molecular weight of 5.0 kg/mol and polydispersity of 1.1 was purchased from Scientific Polymer Products, Inc. Linear PCHMA with number average-molecular weight of 457.5 kg/mol and polydispersity of 1.25 (relative to PS standards) was purchased from Polymer Source, Inc.

Norbornene-Functionalized Poly(cyclohexyl methacrylate) Macromonomer (NBPCHMA). NBPCHMA was synthesized by reversible addition-fragmentation chain transfer (RAFT) polymerization as previously reported with modifications. 45 NBCTA (131.3 mg, 0.258 mmol), CHMA (4.49 mL, 25.8 mmol), and AIBN (0.39 mg, 0.0024 mmol) were dissolved in 6 mL of anhydrous tetrahydrofuran (THF) in a Schlenk tube equipped with a stir bar. Three freeze-pump-thaw cycles were conducted to remove oxygen, and then the tube was heated to 80 °C to start the reaction. During the reaction, aliquots were taken and tested by gel permeation chromatography (GPC) to monitor the molecular weight. After reaching the target molecular weight, the reaction was stopped, and the polymer was precipitated in cold methanol and collected by filtration. After drying in a vacuum oven, the polymer was dissolved in dichloromethane (DCM) and reprecipitated in cold methanol to further purify the macromonomer. These purification steps were repeated three times. Yield: 48.1 wt %. <sup>1</sup>H nuclear magnetic resonance (NMR) and GPC analyses are presented in the Supporting Information, Figures S1 and S2. Number-

average molecular weight and degree of polymerization  $(N_{\rm sc})$  of NBPCHMA calculated from <sup>1</sup>H NMR was 7.87 kg/mol and 43.8, respectively. Molecular weight dispersity of NBPCHMA was 1.25 as determined through refractive index analysis relative to monodisperse PS standards.

Bottlebrush PCHMA (BBPCHMA). BBPCHMA was synthesized in a nitrogen-filled glove box. The predetermined amount of NBPCHMA was added into a vial with a stir bar. Anhydrous DCM was added to the vial targeting a total macromonomer concentration at 0.02 M. Grubbs catalyst was dissolved in the desired amount of anhydrous DCM, and 0.1 mL of the catalyst solution was added into the macromonomer solution (detailed feed ratios of the macromonomer and the catalyst are shown in Table 1). After 5 h, the product was collected by precipitation in cold methanol. GPC analyses are presented in the Supporting Information, Figure S2. The conversion of the macromonomer was estimated through GPC-refractive index (GPC-RI) analysis and is presented in Table 1.

Preparation of PS-Coated Substrate. PS-coated substrates were prepared following a previous report. A Solution of 1 wt hydroxylterminated PS in toluene was spin-coated onto precleaned silicon wafers at 1000 rpm to produce a film of approximately 4 nm thickness. The wafers were then heated under vacuum at 140 °C for 2 days. Unattached polymer chains were removed by repeated rinsing with toluene. Attachment of PS to the surfaces was confirmed through contact angle measurements (Supporting Information, Figure S3).

Film Preparation. BBPCHMA or linear PCHMA were dissolved in chlorobenzene with linear PS at a total composition of 5 wt % solids. The mass ratio of PCHMA to PS was 1:9 in all cases. Films were cast by flow coating polymer blend solutions onto pre-cleaned silicon wafers. The gap height was fixed at 200  $\mu$ m, and 10  $\mu$ L of solution was added into the gap for each film. Film thicknesses ranged from 100 to 200 nm and are provided in the Supporting Information, Table S1. Thermal annealing was performed inside a nitrogen-filled glovebox at 150 °C for 2 days. Characteristics of linear PS used to prepare the thin films are listed in Table 2.

Table 2. Number-Average Molecular Weight  $M_n$ , Degree of Polymerization  $N_m$ , Molecular Weight Dispersity D, and  $N_m/N_{\rm sc}$  for Linear Polystyrene (PS)

polymer	$M_{\rm n}$ (kg/mol)	$N_{ m m}$	Ð	$N_{ m m}/N_{ m sc}$
PS3	3.10	29.8	1.05	0.68
PS17	16.9	162	1.02	3.7
PS59	59.3	570	1.05	13
PS120	120	1152	1.04	26

**Instrumentation.** <sup>1</sup>H Nuclear Magnetic Resonance Spectroscopy. <sup>1</sup>H NMR spectra were measured on Bruker 600 MHz spectrometers. <sup>1</sup>H NMR chemical shifts were reported in ppm relative to internal solvent resonances.

Gel Permeation Chromatography. GPC was performed using an Agilent Technologies 1200 series module with THF at 1 mL/min. The module was equipped with three PSS SDV columns in series (100, 1000, and 10,000 Å pore sizes), an Agilent variable wavelength UV/vis detector, a Wyatt Technology HELEOS II multiangle laser light scattering (MALLS) detector ( $\lambda=658$  nm), and a Wyatt Technology Optilab reX RI detector. The flow rate of mobile phase THF was 1 mL/min at 40 °C. The mass conversion of the BB was determined by comparing integrated RI peak areas for the bottlebrush polymer and macromonomer. Bottlebrush polymer absolute molecular weight was determined by static light scattering, and dn/dc was determined by RI analysis, assuming 100% mass recovery of the bottlebrush polymer.

Polarized Optical Microscopy. Optical micrographs were captured by Zeiss Axioplan2 Polarizing Optical Microscope operating in the reflectance mode.

Atomic Force Microscopy. AFM was performed using an NX20 atomic force microscope. The topography and phase contrast were measured by the tapping mode. The probes were silicon, with a spring

constant of approximately 9 N/m and a resonance frequency of 115 kHz. The parameters used for image acquisition were 1.0 Hz scan frequency, 5  $\mu$ m × 5  $\mu$ m scan size, and 256 × 256 image resolution.

Time-of-Flight Secondary Ion Mass Spectrometry. Positive high mass resolution depth profiling was performed using a ToF-SIMS NCS instrument, which combines a ToF SIMS5 instrument (ION-TOF GmbH, Münster, Germany) and an in situ scanning probe microscope (NanoScan, Switzerland) and is maintained by the Shared Equipment Authority (https://sea.rice.edu) from Rice University. Bunched 30 keV Bi<sub>3</sub><sup>+</sup> ions (with a measured current of 0.2 pA) were used as the primary probe for analysis (scanned area  $100 \times 100 \ \mu \text{m}^2$ ), and sputtering was performed using Ar<sub>1500</sub><sup>+</sup> ions at 10 keV with a typical current around 0.1 nA, rastered area 500  $\times$  500  $\mu$ m<sup>2</sup>. The beams were operated in the non-interlaced mode, alternating two analysis cycles and one sputtering cycle (corresponding to 1.63 s) followed by a pause of 3 s for charge compensation with an electron flood gun. The surface potential and extraction bias were both set to 0 V during charge compensation. During depth profiling, the cycle time was fixed to 200  $\mu$ s (corresponding to m/z = 0-3644 a.m.u mass range).

ToF-SIMS Wedge Crater Analysis. A wedge-crater was created in selected films by sputtering each film using  $Ar_{1500}^{+}$  ions at 10 keV. The total crater area was 350  $\times$  400  $\mu$ m<sup>2</sup> and contained three "steps", each of approximate 10 nm depth. A schematic of the crater is provided in the Supporting Information, Figure S4. In situ topographical analysis of the wedge was performed using an AFM in the ToF-SIMS instrument. AFM line scanning was conducted in the contact mode (scanned line 600  $\mu$ m with 10  $\mu$ m of overlap) with a pixel size of 100 nm using a CDT-FMR probe (purchased by Nanosensors, electrically conductive with a diamond coating and an aluminum backside coating on the cantilever) with a velocity of 15  $\mu$ m/s. Chemical mapping of the crater before and after annealing was performed using a bunched 60 keV Bi<sub>3</sub><sup>2+</sup> ion beam configured for high-lateral resolution (with a measured current of 0.2 pA) over a scanning area of 500  $\times$  500  $\mu$ m<sup>2</sup>. Charge compensation with an electron flood gun was applied during the analysis with a surface potential of 0 V. The cycle time was fixed to 100  $\mu$ s (corresponding to m/z = 0-911a.m.u mass range).

Determination of Depth-Dependent PCHMA Composition in Blend Films. The through-film distribution of PCHMA in blend films was determined through ToF-SIMS measurements. We used C<sub>6</sub>H<sub>11</sub><sup>+</sup>, C<sub>7</sub>H<sub>7</sub><sup>+</sup>, and Si<sup>+</sup> ion signals to track PCHMA, PS, and silicon, respectively. The depth-dependent composition of PCHMA in the linear PS matrix was determined through calibration and measurement of the  $C_6H_{11}^+/C_7H_7^+$  ion-intensity ratio. To calibrate ionintensity ratios, we first measured the  $C_6H_{11}^{\phantom{11}+}/C_7H_7^{\phantom{7}+}$  ion-intensity ratio for a series of as-cast and miscible blends of NBPCHMA ( $M_n$  = 7.87 kg/mol) and PS3 ( $M_n = 3.10 \text{ kg/mol}$ ) at known mass ratios. For each blend, we determined the average  $C_6H_{11}^+/C_7H_7^+$  ion-intensity ratio through ToF-SIMS depth profiling measurements. These ionintensity ratios were found to vary linearly with the NBPCHMA/PS mass ratios. We produced a linear fit of the secondary ion-intensity ratio as a function of NBPCHMA mass composition and used this to determine PCHMA mass concentration based on measured secondary ion-intensity ratios from the blend films studied. The resulting mass compositional distributions were integrated and normalized with respect to the known PCHMA content in each film, 10 wt %. As the linear PS homopolymer contributed some  $C_6H_{11}^+$  ion intensity along with  $C_7H_7^+$  ion intensity, the background C<sub>6</sub>H<sub>11</sub><sup>+</sup> ion intensity was measured for PS homopolymer and subtracted from the measured  $C_6H_{11}^+$  ion intensity from the blend films. Additional details including the secondary ion ratios measured during calibration and the linear relationship between the secondary ion ratio and film composition are provided in the Supporting Information. The measured ion-intensity ratios along with a linear fit to each dataset are presented in the Supporting Information, Figure S5 and Table S2.

Determination of Interfacial Excesses. The surface, substrate, and total excesses were determined through integration of the depth-dependent PCHMA compositions

$$z^* = z_{\text{surf}}^* + z_{\text{sub}}^* = \int_0^{h/2} [\varphi(z) - \varphi^0] dz + \int_{h/2}^0 [\varphi(z) - \varphi^0] dz$$

where surface, substrate, and total excesses are denoted as  $z_{\rm surf}^*$ ,  $z_{\rm sub}^*$ , and  $z^*$ , respectively. h is the thickness of the film, z=0 corresponds to the film—air interface, and z=h designates the film—substrate interface.  $\varphi(z)$  is the mass fraction of PCHMA in the film as a function of depth z.  $\varphi^0$  is taken to be the composition of PCHMA in the middle of the film. The integrations were performed over the surface and substrate regions of the film, which were z=0 to h/2 for the surface and z=h/2 to h for the substrate.

Surface Energy Measurement. The surface energy of polymer melts at 150 °C was measured by the pendant drop method using Krüss Instruments Drop Shape Analyzer DSA 100 equipped with the high temperature and pressure device PD-E1700 MD. Polymer samples with a Kapton spacer were hot-pressed to obtain films with a thickness of 0.5 mm, and pellet samples with 1 cm diameter were cut from these films. The pellet samples were attached to a needle preheated at 150 °C in the measurement chamber. The samples were held at the measurement temperature until they formed a stable pendant drop, and then the surface energy was measured through analysis of the droplet curvature. The chamber was under nitrogen during sample preparation and measurement. The reported surface energies reflected average values from the measurements repeated 200 times with a 1 min interval.

The surface energy of polymers at room temperature was measured by static contact angle measurements with a Drop Shape Analyzer DSA 100. DI water and diiodomethane were used as testing liquids. Contact angles were measured 30 s after the test fluid contacted the surface. The reported contact angles reflected average values with standard deviation from at least ten measurements. Polar and disperse components of surface energy were calculated by the Owens—Wendt–Rabel–Kaelble (OWRK) method. 48,49

## ■ RESULTS AND DISCUSSION

The primary goal of the present study was to determine whether entropic effects would drive surface segregation of bottlebrush polymers in blends with linear polymers with attractive intermolecular interactions. We studied blend films containing 10 wt % bottlebrush polymers with PCHMA sidechains (BBPCHMA) and linear PS. Linear PCHMA and linear PS are miscible and exhibit a negative  $\chi$ -interaction parameter from ambient temperatures up to 220 °C and a lower-critical solution temperature at approximately 240 °C. 41-43 Both polymers have a glass-transition temperature  $T_{\rm g}$  near 105 °C. In our studies of blend films, we varied the degree-ofpolymerization of the linear PS (N<sub>m</sub>) and the degree-ofpolymerization of the BBPCHMA backbone  $(N_b)$ . Prior work by us and others has shown that the ratio  $N_{\rm m}/N_{\rm sc}$  is important for segregation of branched polymer additives to interfaces, and the backbone degree of polymerization for the bottlebrush  $N_{\rm b}$  can also play a role in the segregation of bottlebrush polymers to the free surface.  $^{20,22,23,35-37,50}$   $N_{\rm m}/N_{\rm sc}$  reflects the ratio of chain ends in the bottlebrush to the linear polymer, and the bottlebrush segregation to interfaces generally increases with increasing  $N_{\rm m}/N_{\rm sc}$ . Prior studies have found that segregation increases with increasing  $N_b/N_{sc}$ .

BBPCHMA bottlebrushes were synthesized *via* a "grafting-through" ring opening metathesis polymerization, as shown in Scheme 1. NBPCHMA macromonomers were first synthesized by RAFT using an *exo*-norbornene-functionalized chain transfer agent (CTA). The bottlebrush polymer was subsequently synthesized by ring-opening metathesis polymerization (ROMP). The final macromonomer conversion decreased with increasing target bottlebrush backbone length and ranged from approximately 80–90% (see Table 1). Our

Scheme 1. Synthetic Scheme for Bottlebrush Polymers with PCHMA Side Chains (BBPCHMA)<sup>a</sup>

<sup>a</sup>(i) AIBN, CHMA, THF, 80 °C; (ii) Grubbs catalyst (3rd Gen.), DCM.

previous studies demonstrated that bottlebrush polymers generally segregated more strongly than residual unreacted macromonomers, and the residual macromonomer had little impact on the measured surface segregation behavior of bottlebrush polymers in blend films.<sup>36</sup>

We prepared blend films of BBPCHMA with linear PS. In all blend films studied, the weight fraction of BBPCHMA was 10 wt %. The molecular weight of linear PS was varied to span chain lengths that were both shorter and longer than the BBPCHMA side chains (Table 2). For each blend, we characterized the structure for the as-cast and annealed (2 days at 150 °C) films. Films were analyzed by polarized optical microscopy (Supporting Information, Figure S6) and atomic force microscopy (AFM) (Supporting Information, Figure S7). All samples were optically smooth and exhibited uniform surface morphologies before and after annealing.

We performed ToF-SIMS depth-profiling analysis on all blend films to determine the through-film bottlebrush distribution and detect segregation of bottlebrush polymer at the air surface and silicon substrate. ToF-SIMS is a powerful technique for analyzing the depth-dependent composition of blend films and enables the simultaneous detection of elemental and molecular ion species. We analyzed  $C_7H_7^+$ ,  $C_6H_{11}^+$ , and Si $^+$  secondary ion signals, which corresponded to PS, PCHMA, and Si, respectively. Figure 1 shows the three-dimensional reconstructions of the ToF-SIMS data reflecting the measured ion intensities throughout the thicknesses of the analyzed areas. These false-color images provide a qualitative view of the segregation in the blend films but do not directly reflect the composition of bottlebrush

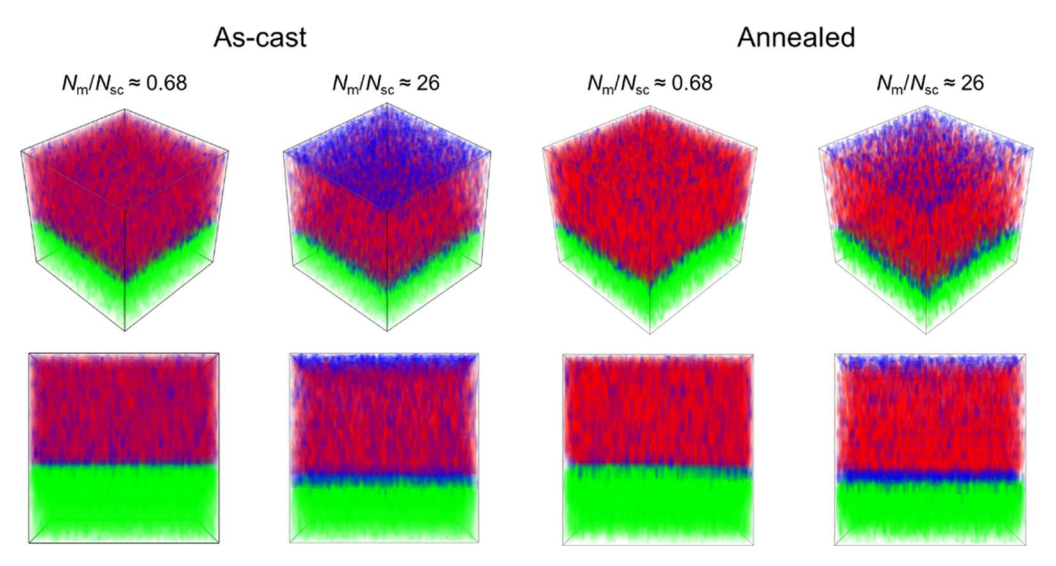


**Figure 1.** ToF-SIMS image maps for as-cast and annealed thin film blends of BBPCHMA-25 with PS3 and PS120. The lateral dimensions of the film areas analyzed are  $100 \times 100 \ \mu m$ . Each color represents a different uncalibrated secondary ion signal:  $C_7H_7^+$  in red,  $C_6H_{11}^+$  in blue, and Si<sup>+</sup> in green, reflecting PS, BBPCHMA, and silicon, respectively.

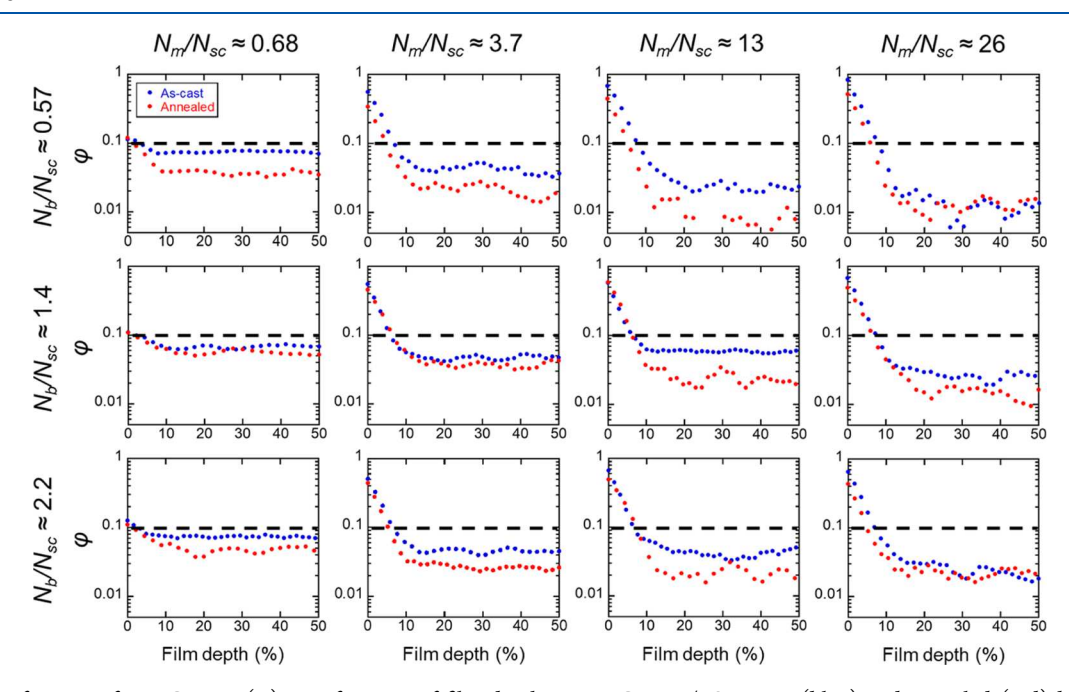


Figure 2. Mass fraction of BBPCHMA ( $\varphi$ ) as a function of film depth in BBPCHMA/PS as-cast (blue) and annealed (red) blend films. The polymer—air interface and middle of the film are at 0 and 50% film depth, respectively. The horizontal dotted line denotes the average mass fraction of BBPCHMA in the blend films (0.1).

because the ion intensities shown are uncalibrated. In the ascast films, BBPCHMA was enriched near the substrate—film interface for both short (PS3) and long (PS120) PS matrices, but enrichment at the free surface (film—air interface) only occurred when in blends with the longer PS chains (PS120). After annealing, there was a slight reduction in the concentration of BBPCHMA near the free surface and increased segregation toward the substrate. The uncalibrated ion-intensity data for all blend film samples as a function of film depth are presented in the Supporting Information, Figure S8.

In Figure 2, we present the depth-dependent mass concentration of bottlebrush polymer for the as-cast (blue) and annealed (red) thin film blends from the polymer-air

interface to the middle of the film. The ion-intensity data were calibrated through analysis of a series of miscible blends of PCHMA and PS of known composition, and details are provided in the Supporting Information. We analyzed bottlebrush segregation to the free surface for different values of  $N_{\rm b}$  and  $N_{\rm m}$ , and we provide values for  $N_{\rm b}/N_{\rm sc}$  and  $N_{\rm m}/N_{\rm sc}$  for each row and column, respectively. We only present depth-dependent compositions from the free surface to the middle of the film because we wish to focus on bottlebrush segregation to the free surface, and plots of the mass distribution throughout the entire film are shown in the Supporting Information, Figure S9.

For the as-cast blends, we observed strong segregation of BBPCHMA to the air—film interface (film depth = 0%) when

 $N_{\rm m}/N_{\rm sc} \geq 3.7$ . In addition, BBPCHMA was increasingly enriched at the surface and depleted from the interior of the film as  $N_{\rm m}/N_{\rm sc}$  increased. For example, for  $N_{\rm b}/N_{\rm sc} \approx 0.57$ , the mass fraction of BBPCHMA at the surface of the film  $(\varphi_{\rm surf})$  increased from 0.12 to 0.84 when  $N_{\rm m}/N_{\rm sc}$  increased from 0.68 to 26. The segregation of BBPCHMA to the surface also depended to some extent on  $N_{\rm b}/N_{\rm sc}$ . For example, for  $N_{\rm m}/N_{\rm sc} \approx 26$ ,  $\varphi_{\rm surf}$  decreased from 0.84 to 0.65 with an increase in  $N_{\rm b}/N_{\rm sc}$  from 0.57 to 2.2. These results show that bottlebrush segregation increases with increasing linear PS size (larger  $N_{\rm m}/N_{\rm sc}$ ) and decreasing bottlebrush size (smaller  $N_{\rm b}/N_{\rm sc}$ ) in the as-cast films.

The blend films were annealed in order to thermally equilibrate the blends, and we chose a temperature of 150 °C because it was above the glass-transition temperature for both PS and PCHMA and within the temperature range of attractive intermolecular interactions. 43 The mass fraction of BBPCHMA at the free surface decreased slightly after thermal annealing, but a strong surface enrichment of BBPCHMA remained for samples with  $N_{\rm m}/N_{\rm sc} \geq$  3.7. For example,  $\varphi_{\rm surf}$  decreased from 0.84 for the as-cast sample to approximately 0.52 after 2 days thermal annealing for blend films with  $N_{\rm m}/N_{\rm sc} \approx 26$  and  $N_{\rm b}/$  $N_{\rm sc} \approx 0.57$ , which is significantly higher than the average blend BBPCHMA weight fraction of 0.10. After annealing, no differences in surface segregation were observed across the series varying in  $N_b/N_{sc}$ . The concentration of BBPCHMA in the interior of all films decreased during annealing, and the concentration of BBPCHMA at the substrate interface increased (Supporting Information, Figure S9).

The surface excesses  $z_{\text{surf}}^*$  for BBPCHMA/PS samples were determined by integrating the bottlebrush mass composition curves from the free surface to the middle of the film, as described in the Experimental Section, and the results are presented in Figure 3. For both the as-cast and annealed

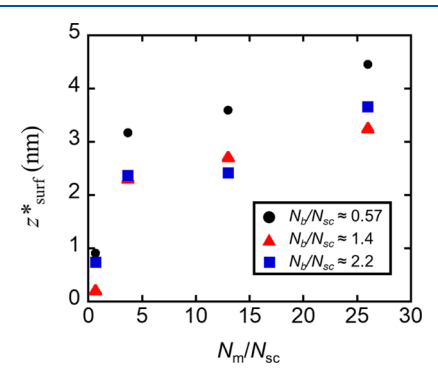


**Figure 3.** Surface excess  $z_{\rm surf}^*$  as a function of  $N_{\rm m}/N_{\rm sc}$  for the as-cast BBPCHMA/PS blends with  $N_{\rm b}/N_{\rm sc}\approx 0.57$  (black circle),  $N_{\rm b}/N_{\rm sc}\approx 1.4$  (red triangle), and  $N_{\rm b}/N_{\rm sc}\approx 2.2$  (blue square).

samples, the surface excess  $z_{\rm surf}^*$  increased with  $N_{\rm m}/N_{\rm sc}$ . The smallest bottlebrush polymer  $(N_{\rm b}/N_{\rm sc}\approx 0.57)$  exhibited stronger surface excess compared with the larger bottlebrush polymers, but only in the as-cast films. After thermal annealing, the difference between the samples with different  $N_{\rm b}/N_{\rm sc}$  values disappears (Supporting Information, Figure S10). This suggests that relative molecular size plays a role in the surface enrichment only during casting. Prior studies on casting behavior of dispersion of size-mismatched colloids reported that accumulation of small colloids at the surface can be observed under fast solvent evaporation.  $^{30,31}$ 

We also studied the effect of the substrate chemistry on the segregation of BBPCHMA additives to both the film—air and film—substrate interfaces. Films were prepared on two types of surfaces: clean Si wafers, which have a thin native oxide layer, and Si wafers coated with a PS brush. For films on Si, the BBPCHMA additives were strongly enriched at the Si substrate (film depth = 100%) for all samples. Full depth profiles for two representative blend films are shown in Figure 4, and full depth

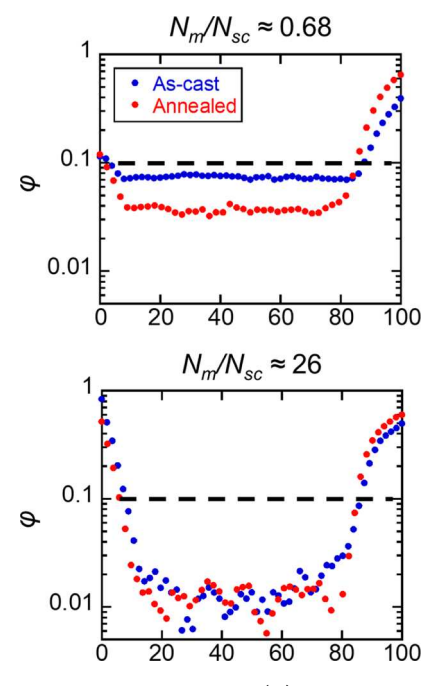


**Figure 4.** Mass fraction of BBPCHMA ( $\varphi$ ) as a function of film depth in (top) BBPCHMA-25/PS3 and (bottom) BBPCHMA-25/PS120 blend films. As-cast and annealed blend films are represented by blue and red points, respectively. The polymer—air interface and polymer—substrate interface of the film are at 0 and 100% film depth, respectively. The horizontal dotted line denotes the average mass fraction of BBPCHMA in the blend films (0.1).

profiles for all films on Si are presented in the Supporting Information, Figure S9. Figure 4 shows that accumulation of BBPCHMA at the substrate was significant for both high and low values of  $N_{\rm m}/N_{\rm sc}$  and in both the as-cast and thermally annealed films. The accumulation of BBPCHMA at the substrate was likely due to attractive interactions between PCHMA and the underlying native oxide. We calculated the substrate excess  $z_{\rm sub}^*$  by integrating the bottlebrush composition from the middle of the film to the substrate.  $z_{\rm sub}^*$  increased with  $N_{\rm m}/N_{\rm sc}$ , and it also increased by annealing, reflecting migration of bottlebrush to the Si substrate (Supporting Information, Figure S10). For films on PS brushes, we prepared blend films of BBPCHMA-62 with all four linear PS polymers listed in Table 2 and analyzed the depth-dependent bottlebrush concentration by ToF-SIMS (Supporting Information, Figures S11 and S12). We found that bottlebrush segregation to the substrate was suppressed after coating the substrate with the PS brush. For  $N_{\rm m}/N_{\rm sc} \le$ 3.7, the bottlebrush was depleted near the substrate and enriched at the film-air interface in the as-cast films. Furthermore, when  $N_{\rm m}/N_{\rm sc} \approx 26$  and  $N_{\rm b}/N_{\rm sc} \approx 1.4$ , the mass fraction of bottlebrush at the substrate interface  $(\varphi_{\text{sub}})$  in the as-cast films was 0.29 on a PS-coated substrate and 0.43 on an unmodified substrate. The concentration of bottlebrush

near the substrate increased after annealing. For example, in the case where  $N_{\rm m}/N_{\rm sc}\approx 26$  and  $N_{\rm b}/N_{\rm sc}\approx 1.4$ ,  $\varphi_{\rm sub}$  for a blend film on a PS-coated substrate increased from 0.29 to 0.39 by annealing, while  $\varphi_{\rm sub}$  for a blend film on an unmodified substrate increased from 0.43 to 0.56. Importantly, the substrate chemistry had little impact on segregation of BBPCHMA to the film—air interface, and no difference of surface enrichment was observed between the thin film blends on PS-coated wafers and unmodified Si wafers. For example, in the case where  $N_{\rm m}/N_{\rm sc}\approx 26$  and  $N_{\rm b}/N_{\rm sc}\approx 1.4$ ,  $\varphi_{\rm surf}$  of the ascast and annealed blends on PS-coated substrates were 0.67 and 0.44 and that for blends on unmodified substrates were 0.68 and 0.48, respectively.

To further understand the effects driving surface segregation of BBPCHMA, we prepared and analyzed blends of linear PCHMA and PS. We chose a linear PCHMA with a molecular weight of 457.5 kg/mol, similar to that of BBPCHMA-62, and prepared blends with the entire series of linear PS (Table 2). ToF-SIMS depth profiling analyses for these samples are provided in the Supporting Information, Figures S13 and S14, and the surface mass fractions of PCHMA are provided in Table 3. We also verified the uniformity of these blends by

Table 3. Mass Fractions of PCHMA at the Free Surface  $\varphi_{\text{surf}}$  for As-Cast BBPCHMA-62/PS and Linear PCHMA/PS Blends<sup>a</sup>

	$arphi_{ ext{surf}}$				
additive	matrix (DP)				
	PS3 (30)	PS17 (160)	PS59 (570)	PS120 (1150)	
BBPCHMA-62	0.11	0.55	0.58	0.68	
linear PCHMA	0.11	0.27	0.32	0.34	

 $^a\mathrm{All}$  blend films contained an average of 10 wt % PCHMA or BBPCHMA in PS.

optical microscopy and AFM, and these data are provided in the Supporting Information, Figures S15 and S16. The linear PCHMA segregated to the surface in PS17, PS69, and PS120, but not in blends with PS3. The mass fraction of PCHMA at the surface increased with increasing PS molecular weight. However, the mass fraction of PCHMA at the surface for linear PCHMA/PS blends was significantly lower than that for BBPCHMA-62/PS blends, as shown in Table 3. For example, in the as-cast films,  $\varphi_{
m surf}$  was 0.34 for linear PCHMA/PS120 blends and 0.68 for BBPCHMA-62/PS120 blends. These results demonstrate that both enthalpic and entropic effects play a role in the segregation of PCHMA or BBPCHMA to the film surface. Enthalpic effects are primarily responsible for driving linear PCHMA to the film surface as the degree of polymerization of the linear PCHMA (approximately 2720) is much higher than all linear PS used in blends (ranging from 30 to 1150). This enrichment is further enhanced by the bottlebrush architecture, as reflected in the larger  $\phi_{ ext{surf}}$  values across the blend films studied.

To further understand the preference for BBPCHMA over PS at a free surface, we measured the surface energies of BBPCHMA-25 and PS-120 both at 150 °C and at room temperature. The surface energy measurements at 150 °C were conducted using the pendant drop method, and measurements at room temperature were conducted by measuring the contact angle of test liquids deposited on the surface of each material. Photographs of representative measurements are presented in

the Supporting Information, Figures S17 and S18. Table 4 shows surface energies of PS120 and BBPCHMA-25 at 25 and

Table 4. Surface Energy Values of PS120 and BBPCHMA-25 at 25 and 150  $^{\circ}\text{C}$ 

	surface free energy $\left(mN/m\right)$		
polymer	25 °C	150 °C	
PS120	$41.3 \pm 0.08$	$31.8 \pm 0.23$	
BBPCHMA-25	$41.4 \pm 0.12$	$29.2 \pm 0.19$	
PCHMA	40.99 + 0.14	N.A. <sup>a</sup>	

<sup>a</sup>Measurement failed due to the high viscosity of the PCHMA sample  $(M_n = 458 \text{ kg/mol})$ .

150 °C. The measured surface energies of PS are in good agreement with the previously reported values. 53,54 measured surface energy for BBPCHMA at 150 °C (29.2 mN/m) was lower than that of linear PS (31.8 mN/m), and this is consistent with the observed surface layer of BPCHMA additives that remain enriched at the film-air surface after annealing. At the same time, the measured surface energies for BBPCHMA (41.4 mN/m) and linear PS (41.3 mN/m) were within experimental error of each other at room temperature. These room-temperature surface energy measurements were conducted for glassy films and are therefore unlikely to reflect the relevant effects that drive surface segregation during casting or annealing. The measured surface energies at room temperature for linear PS, BBPCHMA, and linear PCHMA are the same, within experimental error (see the Supporting Information, Table S3).

We can compare the results described in this study with prior studies of bottlebrush polymer blends and linear polymers with approximately neutral and repulsive intermolecular interactions. Specifically, we previously studied bottlebrushes with perdeuterated PS side-chains (BBdPS) blended with linear PS. 36 This blend involved approximately neutral (athermal) interactions between the bottlebrush and linear polymer. We also studied bottlebrushes that contained both PS and poly(methyl methacrylate) (PMMA) side-chains (BB(PS-m-PMMA)) blended with linear PS.<sup>35</sup> This system involved repulsive interactions between the bottlebrush and linear PS. To compare the neutral, repulsive, and attractive blends, we selected experiments where  $N_{\rm m}/N_{\rm sc}$  was greater than 10 and  $N_b/N_{sc}$  ranged from 0.9 to 1.4. In the as-cast films,  $\varphi_{
m surf}$  was 0.6 for blends with attractive intermolecular interactions, 0.9 for athermal blends, and 1.0 for blends with repulsive interactions. This comparison shows that repulsive intermolecular interactions between the bottlebrush and linear polymer matrix increase the surface segregation of bottlebrush polymer in the as-cast films, while attractive interactions suppress the surface segregation relative to the other blends. However, after thermal annealing, BBPCHMA exhibited a much higher surface mass fraction ( $\varphi_{\text{surf}} = 0.5$ ) than either BBdPS or BB(PS-m-PMMA), which had surface mass fractions less than 0.3 after annealing. This likely reflects the lower surface energy of PCHMA relative to PS, which results in a stronger preference for the BBPCHMA additives at the surface. For the other cases, enthalpic interactions with the interface were repulsive toward the bottlebrush additive, including the BB(PS-m-PMMA) (relative to PS) and BBdPS (relative to

These results suggest that during casting, the extent of surface enrichment is largely controlled by two attributes: the

architectures of bottlebrush and linear polymers and the enthalpic interactions between bottlebrush and linear polymers. Enthalpic interactions between each polymer and the air surface are less important and are possibly screened by the solvent vapor in equilibrium with the drying film. During thermal annealing, enthalpic interactions of the additives and linear polymer with air play a more important role in determining the surface enrichment. As a result, bottlebrush additives that are strongly enriched at the surface after casting may diffuse back into the film after thermal annealing depending on surface energy of bottlebrushes, reducing the surface enrichment and becoming depleted at the film—air interface. This is shown schematically in Figure 5 and is indeed observed for both BB(PS-m-PMMA) in PS<sup>35</sup> and BBdPS in PS,<sup>36</sup> and to a lesser extent for BBPCHMA in PS.

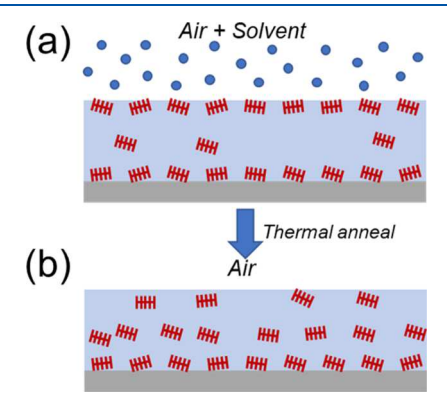
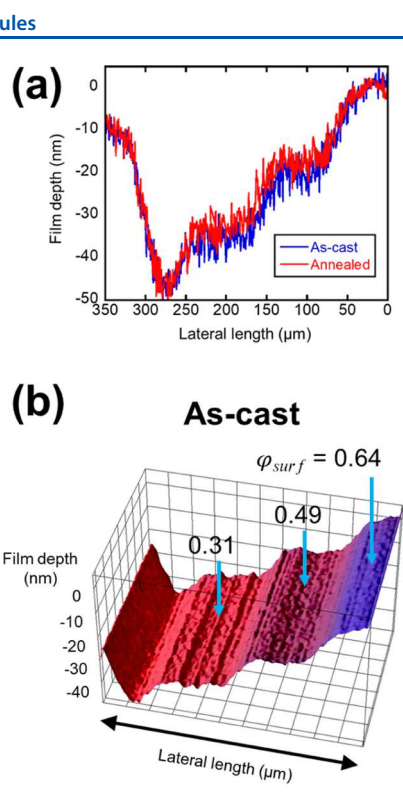
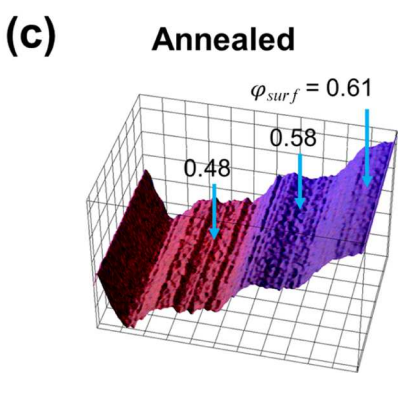


Figure 5. Schematic for the distribution of a bottlebrush polymer that has repulsive interactions with the film—air interface (a) during casting and (b) during thermal annealing. During casting, the solvent vapor screens interactions between the bottlebrush and air, and segregation is driven by architectural effects and enthalpic interactions between the bottlebrush and polymer matrix. During thermal annealing, repulsive interactions with the air interface become important and, in cases where the film—air interface is more strongly repulsive toward the bottlebrush, drive diffusion of the bottlebrush back into the blend film.

Finally, we studied the capability for the surface enrichment of bottlebrush polymers to "self-heal" after damage to the surface. This property would be relevant to the development of robust film coatings that can maintain a desired surface property even after damage. 55-58 The BBPCHMA additives have attractive interactions with PS, and therefore there is a supply of BBPCHMA from the bulk film. The BBPCHMA are also strongly attracted to the film surface due to both enthalpic and entropic effects. We therefore hypothesized that, under thermal annealing, bottlebrush additives in the film could diffuse to "heal" a damaged surface depleted of BBPCHMA. To study this, we prepared a BBPCHMA-25/PS120  $(N_m/N_{sc})$  $\approx 26$ ,  $N_{\rm b}/N_{\rm sc} \approx 0.57$ ) blend film by casting as described above and without thermal annealing. The total thickness of the film was 152 nm. Next, we damaged the surface to create a "wedge crater" by etching into the film at different depths using the Ar<sub>1500</sub><sup>+</sup> ion cluster beam in the ToF-SIMS instrument. We used in situ AFM to quantify the depth of the wedge steps and verify that the topography did not change with thermal annealing, as shown Figure 6a. The wedge crater was made up of three different wedge steps of approximately 16, 32, and 50 nm in depth. The overall lateral length of the wedge crater was approximately 300  $\mu$ m, and the lateral length of each step was





**Figure 6.** Analysis of wedge topography through AFM (a) and 3D surface composition images for ToF-SIMS wedge crater analyses of BBPCHMA-25/PS120k as-cast (b) and annealed at 150 °C for 2 days (c). For the 3D images, secondary ions from PCHMA  $(C_6H_{11}^+)$  and PS  $(C_7H_7^+)$  are represented by blue and red, respectively.

100  $\mu$ m. The composition of BBPCHMA at the surface was determined through ToF-SIMS by measuring the secondary ion-intensity ratios for BBPCHMA ( $C_6H_{11}^+$ ) and PS ( $C_7H_7^+$ ). The results of ToF-SIMS analysis combined with the surface topography from AFM are shown in Figure 6b,c, and twodimensional surface composition images showing a top-down view of ion intensities corresponding to PS and BBPCHMA are presented in the Supporting Information, Figure S19. Before annealing, the surface of the wedge cut was depleted of BBPCHMA, as expected. After annealing at 150 °C for 2 days, the concentration of BBPCHMA almost completely recovered for the 16 and 32 nm etches, demonstrating the ability for damage to the surface to self-heal with annealing. The BBPCHMA composition only partially recovered for the 50 nm etch, reflecting an insufficient supply of bottlebrush from the bulk or surrounding film to diffuse to the damaged surface.

In order to understand this self-healing behavior, we used a simple analysis based on the Stokes-Einstein relation to

estimate the diffusivity of the PCHMA bottlebrush in the linear PS matrix. The viscosity of linear PS  $(1.4 \times 10^5 \text{ Pa s})^{59}$  and size of the BBPCHMA (40 nm)<sup>60</sup> were estimated from prior measurements in the literature. Based on these values and an annealing temperature of 150 °C, the diffusivity of the bottlebrush was estimated to be on the order of 10<sup>-20</sup> to  $10^{-19}$  m<sup>2</sup>/s. If the bottlebrush were to diffuse laterally across the top of the film over an approximate distance of 50  $\mu$ m, this would require an unreasonable amount of time  $(10^6 \text{ to } 10^7 \text{ h})$ . Conversely, if the bottlebrush diffused to the surface from the interior of the film over an estimated distance of 50 nm, the time required would be on the order of 10 h, which was approximately the thermal annealing time used in our experiments. This simple analysis suggests that the film selfheals due to the diffusion of bottlebrush from the bulk film rather than laterally from undamaged regions of the surface. However, we note that the diffusive behavior of the bottlebrushes in linear PS likely deviates from that predicted by the Stokes-Einstein relation due to concentration effects, effects arising from the relative sizes of the bottlebrush and linear PS, and interactions between the bottlebrush and linear PS. For example, prior experiments and simulations of nanoparticles diffusing in polymer liquids have found that deviations from the Stokes-Einstein relation are strongly dependent on the sizes of both polymer and particle. 61-64

#### CONCLUSIONS

We studied the depth-dependent concentration in blends of BBPCHMA and linear PS with variations in the degree of polymerization of bottlebrush backbone  $N_{\rm b}$  and the molecular weight of the linear polymer  $N_{\rm m}$ . We found that the bottlebrush polymer segregated to the film-air interfaces for  $N_{\rm m}/N_{\rm sc} \geq 3.7$ , and the surface enrichment decreased only slightly after thermal annealing. The surface concentration of BBPCHMA additives were significantly higher than that for linear PCHMA additives, demonstrating that the bottlebrush architecture enhances surface enrichment. Bottlebrush segregation to the substrate depended strongly on substrate chemistry, but the substrate chemistry did not have a significant impact on the bottlebrush enrichment at the film-air interface. Surface energy measurements showed that BBPCHMA had a lower surface energy than linear PS at elevated temperatures, and as a result, the BBPCHMA formed a thermally stable surface layer in blends with linear PS. We performed comparisons of the surface concentration for bottlebrush additives with repulsive, approximately neutral, and attractive interactions with linear PS and found that, in the as-cast films, the surface concentration was highest in the repulsive system and lowest in the attractive system. However, for thermally annealed films, the repulsive system studied exhibited the highest relative surface concentration. We attributed this to the interactions between the bottlebrush and the film-air interface, which become more important during thermal annealing. Finally, we demonstrated that BBPCHMA additives could heal a damaged surface under thermal annealing by diffusing to the damaged site on the film. This work provides new insight into the segregation behavior of bottlebrush polymer additives and factors that drive segregation during casting and thermal annealing.

## ASSOCIATED CONTENT

# Supporting Information

The Supporting Information is available free of charge at https://pubs.acs.org/doi/10.1021/acs.macromol.0c00744.

<sup>1</sup>H NMR and GPC characterization data, optical microscopy and AFM analysis of polymer films, polymer film thickness, details on methods for ToF-SIMS calibration, calibrated and uncalibrated full depth profiles for all blends, surface excess and substrate excess for all BBPCHMA/PS blends, contact angle data, pendant drop data, and wedge crater analysis data (PDF)

## AUTHOR INFORMATION

### **Corresponding Authors**

Gila E. Stein — Department of Chemical and Biomolecular Engineering, University of Tennessee, Knoxville, Tennessee 37996; orcid.org/0000-0002-3973-4496; Email: gstein4@utk.edu

Rafael Verduzco — Department of Chemical and Biomolecular Engineering and Department of Materials Science and NanoEngineering, Rice University, Houston, Texas 77005, United States; orcid.org/0000-0002-3649-3455; Email: rafaelv@rice.edu

#### **Authors**

Kazuma Miyagi — Department of Applied Life Science, Faculty of Applied Biological Sciences, Gifu University, Gifu 501-1193, Japan; Department of Chemical and Biomolecular Engineering, Rice University, Houston, Texas 77005, United States; orcid.org/0000-0002-0112-3024

Hao Mei — Department of Chemical and Biomolecular Engineering, Rice University, Houston, Texas 77005, United States

Tanguy Terlier − SIMS Lab, Shared Equipment Authority, Rice University, Houston, Texas 77005, United States; orcid.org/0000-0002-4092-0771

Complete contact information is available at: https://pubs.acs.org/10.1021/acs.macromol.0c00744

#### Notes

The authors declare no competing financial interest.

## ACKNOWLEDGMENTS

K.M. acknowledges support from the Research Fellowship for Young Scientists (DC2, 19J11351) provided by Japan Society for the Promotion of Science (JSPS). H.M. and R.V. acknowledge support from National Science Foundation under grant nos. CMMI-1563008 and CMMI-1934045, Welch Foundation under grant no. C-1888, and the NSF Nanosystems Engineering Research Center for Nanotechnology-Enabled Water Treatment (EEC-1449500). G.E.S. acknowledges support from National Science Foundation under grant no. CMMI-1727517. ToF-SIMS measurements were supported by the National Science Foundation under grant no. CBET-1626418. ToF-SIMS analyses were carried out with support provided by the Shared Equipment Authority at Rice University. We acknowledge Krüss and Eurotechnica GmbH for access to instrumentation for surface energy measurements through the academic partners program.

#### REFERENCES

- (1) Sugimoto, S.; Oda, Y.; Hirata, T.; Matsuyama, R.; Matsuno, H.; Tanaka, K. Surface Segregation of a Branched Polymer with Hydrophilic Poly[2-(2-Ethoxy)Ethoxyethyl Vinyl Ether] Side Chains. *Polym. Chem.* **2017**, *8*, 505–510.
- (2) Irvine, D. J.; Ruzette, A.-V. G.; Mayes, A. M.; Griffith, L. G. Nanoscale Clustering of RGD Peptides at Surfaces Using Comb Polymers. 2. Surface Segregation of Comb Polymers in Polylactide. *Biomacromolecules* **2001**, *2*, 545–556.
- (3) Walton, D. G.; Soo, P. P.; Mayes, A. M.; Sofia Allgor, S. J.; Fujii, J. T.; Griffith, L. G.; Ankner, J. F.; Kaiser, H.; Johansson, J.; Smith, G. D.; Barker, J. G.; Satija, S. K. Creation of Stable Poly(Ethylene Oxide) Surfaces on Poly(Methyl Methacrylate) Using Blends of Branched and Linear Polymers. *Macromolecules* 1997, 30, 6947–6956.
- (4) Kang, J.; Shin, N.; Jang, D. Y.; Prabhu, V. M.; Yoon, D. Y. Structure and Properties of Small Molecule-Polymer Blend Semiconductors for Organic Thin Film Transistors. *J. Am. Chem. Soc.* **2008**, *130*, 12273–12275.
- (5) Wei, Q.; Tajima, K.; Tong, Y.; Ye, S.; Hashimoto, K. Surface-Segregated Monolayers: A New Type of Ordered Monolayer for Surface Modification of Organic Semiconductors. *J. Am. Chem. Soc.* **2009**, *131*, 17597–17604.
- (6) Clark, M. D.; Jespersen, M. L.; Patel, R. J.; Leever, B. J. Predicting Vertical Phase Segregation in Polymer-Fullerene Bulk Heterojunction Solar Cells by Free Energy Analysis. *ACS Appl. Mater. Interfaces* **2013**, *5*, 4799–4807.
- (7) Nishizawa, K.; Konno, T.; Takai, M.; Ishihara, K. Bioconjugated Phospholipid Polymer Biointerface for Enzyme-Linked Immunosorbent Assay. *Biomacromolecules* **2008**, *9*, 403–407.
- (8) Takasu, K.; Kushiro, K.; Hayashi, K.; Iwasaki, Y.; Inoue, S.; Tamechika, E.; Takai, M. Polymer Brush Biointerfaces for Highly Sensitive Biosensors That Preserve the Structure and Function of Immobilized Proteins. *Sens. Actuators, B* **2015**, *216*, 428–433.
- (9) Zhao, H.; Zhu, B.; Luo, S.-C.; Lin, H.-A.; Nakao, A.; Yamashita, Y.; Yu, H.-h. Controlled Protein Absorption and Cell Adhesion on Polymer-Brush-Grafted Poly(3,4-Ethylenedioxythiophene) Films. ACS Appl. Mater. Interfaces 2013, 5, 4536—4543.
- (10) Banquy, X.; Burdyńska, J.; Lee, D. W.; Matyjaszewski, K.; Israelachvili, J. Bioinspired Bottle-Brush Polymer Exhibits Low Friction and Amontons-like Behavior. *J. Am. Chem. Soc.* **2014**, *136*, 6199–6202.
- (11) Ishikawa, T.; Kobayashi, M.; Takahara, A. Macroscopic Frictional Properties of Poly(1-(2-Methacryloyloxy)Ethyl-3- Butyl Imidazolium Bis(Trifluoromethanesulfonyl)-Imide) Brush Surfaces in an Ionic Liquid. ACS Appl. Mater. Interfaces 2010, 2, 1120–1128.
- (12) Zhang, Q.; Archer, L. A. Step-growth synthesis and interfacial friction properties of surface dendron coatings. *Langmuir* **2006**, 22, 717–722.
- (13) Pan, Z.; Peng, R.; Tang, J.; Chen, L.; Cheng, F.; Zhao, B. Surface-Segregation-Induced Nanopapillae on FDTS-Blended PDMS Film and Implications in Wettability, Adhesion, and Friction Behaviors. ACS Appl. Mater. Interfaces 2018, 10, 7476—7486.
- (14) Stein, G. E.; Laws, T. S.; Verduzco, R. Tailoring the Attraction of Polymers toward Surfaces. *Macromolecules* **2019**, *52*, 4787–4802.
- (15) Iyengar, D. R.; Perutz, S. M.; Dai, C.-A.; Ober, C. K.; Kramer, E. J. Surface Segregation Studies of Fluorine-Containing Diblock Copolymers. *Macromolecules* **1996**, *29*, 1229–1234.
- (16) Affrossman, S.; Bertrand, P.; Hartshorne, M.; Kiff, T.; Leonard, D.; Pethrick, R. A.; Richards, R. W. Surface Segregation in Blends of Polystyrene and Perfluorohexane Double End Capped Polystyrene Studied by Static SIMS, ISS, and XPS. *Macromolecules* **1996**, 29, 5432–5437.
- (17) Hariharan, A.; Kumar, S. K.; Russell, T. P. Surface Segregation in Binary Polymer Mixtures: A Lattice Model. *Macromolecules* **1991**, 24, 4909–4917.
- (18) Hariharan, A.; Kumar, S. K.; Rafailovich, M. H.; Sokolov, J.; Zheng, X.; Duong, D.; Schwarz, S. A.; Russell, T. P. The Effect of Finite Film Thickness on the Surface Segregation in Symmetric Binary Polymer Mixtures. *J. Chem. Phys.* **1993**, *99*, 656–663.

- (19) Qian, Z.; Minnikanti, V. S.; Sauer, B. B.; Dee, G. T.; Kampert, W. G.; Archer, L. A. Surface Tension of Polystyrene Blends: Theory and Experiment. J. Polym. Sci. Part B Polym. Phys. 2009, 47, 1666—1685
- (20) Lee, J. S.; Lee, N.-H.; Peri, S.; Foster, M. D.; Majkrzak, C. F.; Hu, R.; Wu, D. T. Surface Segregation Driven by Molecular Architecture Asymmetry in Polymer Blends. *Phys. Rev. Lett.* **2014**, *113*, 225702.
- (21) Fredrickson, G. H.; Liu, A. J.; Bates, F. S. Entropic Corrections to the Flory-Huggins Theory of Polymer Blends: Architectural and Conformational Effects. *Macromolecules* **1994**, 27, 2503–2511.
- (22) Wu, D. T.; Fredrickson, G. H. Effect of Architecture in the Surface Segregation of Polymer Blends. *Macromolecules* **1996**, 29, 7919–7930.
- (23) Walton, D. G.; Mayes, A. M. Entropically Driven Segregation in Blends of Branched and Linear Polymers. *Phys. Rev. E: Stat. Phys., Plasmas, Fluids, Relat. Interdiscip. Top.* **1996**, 54, 2811–2815.
- (24) Hariharan, A.; Kumar, S. K.; Russell, T. P. A Lattice Model for the Surface Segregation of Polymer Chains Due to Molecular Weight Effects. *Macromolecules* **1990**, *23*, 3584–3592.
- (25) Matsen, M. W.; Mahmoudi, P. Segregation of Chain Ends to the Surface of a Polymer Melt. Eur. Phys. J. E 2014, 37, 1–8.
- (26) Wu, D. T.; Fredrickson, G. H.; Carton, J.-P.; Ajdari, A.; Leibler, L. Distribution of Chain Ends at the Surface of a Polymer Melt: Compensation Effects and Surface Tension. *J. Polym. Sci. Part B Polym. Phys.* **1995**, 33, 2373–2389.
- (27) Minnikanti, V. S.; Archer, L. A. Entropic Attraction of Polymers toward Surfaces and Its Relationship to Surface Tension. *Macromolecules* **2006**, *39*, 7718–7728.
- (28) Jacobs, M.; Liang, H.; Pugnet, B.; Dobrynin, A. V. Molecular Dynamics Simulations of Surface and Interfacial Tension of Graft Polymer Melts. *Langmuir* **2018**, 34, 12974–12981.
- (29) Donley, J. P.; Fredrickson, G. H. Influence of Conformational Asymmetry on the Surface Enrichment of Polymer Blends II. *J. Polym. Sci. Part B Polym. Phys.* **1995**, *33*, 1343–1351.
- (30) Zhou, J.; Man, X.; Jiang, Y.; Doi, M. Structure Formation in Soft-Matter Solutions Induced by Solvent Evaporation. *Adv. Mater.* **2017**, 29, 1703769.
- (31) Zhou, J.; Jiang, Y.; Doi, M. Cross Interaction Drives Stratification in Drying Film of Binary Colloidal Mixtures. *Phys. Rev. Lett.* **2017**, *118*, 108002.
- (32) Howard, M. P.; Nikoubashman, A.; Panagiotopoulos, A. Z. Stratification in Drying Polymer-Polymer and Colloid-Polymer Mixtures. *Langmuir* **2017**, 33, 11390–11398.
- (33) Cheng, S.; Grest, G. S. Dispersing Nanoparticles in a Polymer Film via Solvent Evaporation. ACS Macro Lett. **2016**, *5*, 694–698.
- (34) Cummings, J.; Lowengrub, J. S.; Sumpter, B. G.; Wise, S. M.; Kumar, R. Modeling Solvent Evaporation during Thin Film Formation in Phase Separating Polymer Mixtures. *Soft Matter* **2018**, *14*, 1833–1846.
- (35) Mei, H.; Laws, T. S.; Mahalik, J. P.; Li, J.; Mah, A. H.; Terlier, T.; Bonnesen, P.; Uhrig, D.; Kumar, R.; Stein, G. E.; Verduzco, R. Entropy and Enthalpy Mediated Segregation of Bottlebrush Copolymers to Interfaces. *Macromolecules* **2019**, *52*, 8910.
- (36) Mah, A. H.; Laws, T.; Li, W.; Mei, H.; Brown, C. C.; Ievlev, A.; Kumar, R.; Verduzco, R.; Stein, G. E. Entropic and Enthalpic Effects in Thin Film Blends of Homopolymers and Bottlebrush Polymers. *Macromolecules* **2019**, *52*, 1526–1535.
- (37) Mitra, I.; Li, X.; Pesek, S. L.; Makarenko, B.; Lokitz, B. S.; Uhrig, D.; Ankner, J. F.; Verduzco, R.; Stein, G. E. Thin Film Phase Behavior of Bottlebrush/Linear Polymer Blends. *Macromolecules* **2014**, *47*, 5269–5276.
- (38) Pesek, S. L.; Lin, Y.-H.; Mah, H. Z.; Kasper, W.; Chen, B.; Rohde, B. J.; Robertson, M. L.; Stein, G. E.; Verduzco, R. Synthesis of Bottlebrush Copolymers Based on Poly(Dimethylsiloxane) for Surface Active Additives. *Polymer* **2016**, *98*, 495–504.
- (39) Mah, A. H.; Afzali, P.; Qi, L.; Pesek, S.; Verduzco, R.; Stein, G. E. Bottlebrush Copolymer Additives for Immiscible Polymer Blends. *Macromolecules* **2018**, *51*, 5665–5675.

- (40) Yethiraj, A. Entropic and Enthalpic Surface Segregation from Blends of Branched and Linear Polymers. *Phys. Rev. Lett.* **1995**, *74*, 2018–2021.
- (41) Harton, S. E.; Koga, T.; Stevie, F. A.; Araki, T.; Ade, H. Investigation of Blend Miscibility of a Ternary PS/PCHMA/PMMA System Using SIMS and Mean-Field Theory. *Macromolecules* **2005**, 38, 10511–10515.
- (42) Friedrich, C.; Schwarzwälder, C.; Riemann, R.-E. Rheological and Thermodynamic Study of the Miscible Blend Polystyrene/Poly(Cyclohexyl Methacrylate). *Polymer* 1996, 37, 2499–2507.
- (43) Pomposo, J. A.; Múgica, A.; Aréizaga, J.; Cortázar, M. Modeling of the Phase Behavior of Binary and Ternary Blends Involving Copolymers of Styrène, Methyl Methacrylate and Cyclohexyl Methacrylate. *Acta Polym.* **1998**, *49*, 301–311.
- (44) Radzinski, S. C.; Foster, J. C.; Matson, J. B. Preparation of Bottlebrush Polymers via a One-Pot Ring-Opening Polymerization (ROP) and Ring-Opening Metathesis Polymerization (ROMP) Grafting-Through Strategy. *Macromol. Rapid Commun.* **2016**, 37, 616–621.
- (45) Radzinski, S. C.; Foster, J. C.; Chapleski, R. C.; Troya, D.; Matson, J. B. Bottlebrush Polymer Synthesis by Ring-Opening Metathesis Polymerization: The Significance of the Anchor Group. *J. Am. Chem. Soc.* **2016**, *138*, 6998–7004.
- (46) Mansky, P.; Liu, Y.; Huang, E.; Russell, T. P.; Hawker, C. Controlling Polymer-Surface Interactions with Random Copolymer Brushes. *Science* **1997**, 275, 1458–1460.
- (47) Mah, A. H.; Mei, H.; Basu, P.; Laws, T. S.; Ruchhoeft, P.; Verduzco, R.; Stein, G. E. Swelling Responses of Surface-Attached Bottlebrush Polymer Networks. *Soft Matter* **2018**, *14*, 6728–6736.
- (48) Kaelble, D. H. Dispersion-Polar Surface Tension Properties of Organic Solids. *J. Adhes.* **1970**, *2*, 66–81.
- (49) Owens, D. K.; Wendt, R. C. Estimation of the Surface Free Energy of Polymers. *J. Appl. Polym. Sci.* **1969**, *13*, 1741–1747.
- (50) Sun, F. C.; Dobrynin, A. V.; Shirvanyants, D.; Lee, H. II; Matyjaszewski, K.; Rubinstein, G. J.; Rubinstein, M.; Sheiko, S. S. Flory Theorem for Structurally Asymmetric Mixtures. *Phys. Rev. Lett.* **2007**, *99*, 137801.
- (51) Winograd, N. Imaging Mass Spectrometry on the Nanoscale with Cluster Ion Beams. *Anal. Chem.* **2015**, *87*, 328–333.
- (52) Terlier, T.; Zappalà, G.; Marie, C.; Leonard, D.; Barnes, J.-P.; Licciardello, A. ToF-SIMS Depth Profiling of PS-b-PMMA Block Copolymers Using Arn+, C60++, and Cs+ Sputtering Ions. *Anal. Chem.* **2017**, *89*, 6984–6991.
- (53) Wu, S. Surface and Interfacial Tensions of Polymer Melts. II. Poly(Methyl Methacrylate), Poly(n-Butyl Methacrylate), and Polystyrene. *J. Phys. Chem.* **1970**, *74*, 632–638.
- (54) Qian, Ż.; Minnikanti, V. S.; Sauer, B. B.; Dee, G. T.; Archer, L. A. Surface Tension of Symmetric Star Polymer Melts. *Macromolecules* **2008**, *41*, 5007–5013.
- (55) Liu, Q.; Wang, X.; Yu, B.; Zhou, F.; Xue, Q. Self-Healing Surface Hydrophobicity by Consecutive Release of Hydrophobic Molecules from Mesoporous Silica. *Langmuir* **2012**, 28, 5845–5849.
- (56) Zhou, H.; Wang, H.; Niu, H.; Zhao, Y.; Xu, Z.; Lin, T. A Waterborne Coating System for Preparing Robust, Self-Healing, Superamphiphobic Surfaces. *Adv. Funct. Mater.* **2017**, 27, 1604261.
- (57) Wang, H.; Xue, Y.; Ding, J.; Feng, L.; Wang, X.; Lin, T. Durable, Self-Healing Superhydrophobic and Superoleophobic Surfaces from Fluorinated-Decyl Polyhedral Oligomeric Silsesquioxane and Hydrolyzed Fluorinated Alkyl Silane. *Angew. Chem., Int. Ed.* **2011**, *50*, 11433–11436.
- (58) Li, B.; Zhang, J. Durable and Self-Healing Superamphiphobic Coatings Repellent Even to Hot Liquids. *Chem. Commun.* **2016**, *52*, 2744–2747.
- (59) Fox, T. G., Jr; Flory, P. J. Viscisty-Molecular Weight and Viscosity-Temperature Relationships for Polystyrene and Polyisobutylene. J. Am. Chem. Soc. 1948, 70, 2384–2395.
- (60) Pesek, S. L.; Li, X.; Hammouda, B.; Hong, K.; Verduzco, R. Small-Angle Neutron Scattering Analysis of Bottlebrush Polymers

- Prepared via Grafting-Through Polymerization. *Macromolecules* **2013**, 46, 6998–7005.
- (61) Tuteja, A.; Mackay, M. E.; Narayanan, S.; Asokan, S.; Wong, M. S. Breakdown of the Continuum Stokes-Einstein Relation for Nanoparticle Diffusion. *Nano Lett.* **2007**, *7*, 1276–1281.
- (62) Lurio, L. B.; Lumma, D.; Sandy, A. R.; Borthwick, M. A.; Falus, P.; Mochrie, S. G. J.; Pelletier, J. F.; Sutton, M.; Regan, L.; Malik, A.; Stephenson, G. B. Absence of Scaling for the Intermidiate Scattering Function of a Hard-Sphere Suspension: Static and Dynamic X-Ray Scattering from Concentrated Polystyrene Latex Spheres. *Phys. Rev. Lett.* **2000**, 84, 785–788.
- (63) Ganesan, V.; Pryamitsyn, V.; Surve, M.; Narayanan, B. Noncontinuum effects in nanoparticle dynamics in polymers. *J. Chem. Phys.* **2006**, *124*, 221102.
- (64) Wyart, F. B.; de Gennes, P. G. Viscosity at small scales in polymer melts. Eur. Phys. J. E 2000, 1, 93–97.